Available online at www.sciencedirect.com
SCIENCE DIRECT®
Journal of Chromatography A, 988 (2003) 185–203
JOURNAL OF CHROMATOGRAPHY A
www.elsevier.com/locate/chroma

Determination of single component isotherms and affinity energy distribution by chromatography

Fabrice Gritti[a,b], Gustaf Gotmar[a,b], Brett J. Stanley[c], Georges Guiochon[a,b,*]

[a]*Department of Chemistry, The University of Tennessee, Knoxville, TN 37996-1600, USA*
[b]*Division of Chemical Sciences, Oak Ridge National Laboratory, Oak Ridge, TN, USA*
[c]*Department of Chemistry, California State University, San Bernardino, CA 92407, USA*

Received 21 October 2002; received in revised form 18 December 2002; accepted 19 December 2002

Abstract

Adsorption isotherm data were acquired by frontal analysis (FA) and large sample-size band profiles were recorded for phenol and caffeine. For both compounds, the isotherm data fit well to the Langmuir, Toth, and Bi-Langmuir models of adsorption. The Langmuir model must be dismissed because it does not predict accurately the overloaded band profiles. However, profiles calculated using the unimodal Toth and the bimodal Bi-Langmuir models are indistinguishable. The expectation-maximization procedure was used to calculate directly the affinity energy distribution (AED) from the raw FA data points. For both compounds, the AED converges to a bimodal distribution at high numbers of iterations. This result, which shows the high sensitivity of the EM method, suggest that the Bi-Langmuir model makes better physical sense than the Toth model. This model also permits a detailed investigation of the properties of active sites, a feature often evoked in chromatography but so far rarely the topic of a quantitative investigation.
© 2003 Elsevier Science B.V. All rights reserved.

Keywords: Adsorption isotherms; Frontal analysis; Adsorption energy distributions; Mathematical modelling; Caffeine; Phenols

1. Introduction

The rapid development of the applications of preparative liquid chromatography in the pharmaceutical industry has led to the recent renewal of interest in the fundamentals of nonlinear chromatography [1,2]. It has become possible to calculate the optimum design and operating conditions of a separation [1,3]. However, this calculation requires a prior accurate understanding of the thermodynamics and the kinetics of the chromatographic process involved in the separation studied. The former is characterized by the competitive isotherms of the feed components, the latter by the rate coefficients of the various steps involved in mass transfer across the column [1,2].

It was demonstrated that thermodynamics controls band profiles, particularly at high concentrations and when the mass transfer kinetics is not very slow [1]. Accordingly, it determines, to a large extent, the recovery yield and production rate that any industrial unit can achieve. For obvious economic reasons,

*Corresponding author. Tel.: +1-865-974-0733; fax: +1-865-974-2667.
E-mail address: guiochon@novell.chem.utk.edu (G. Guiochon).

0021-9673/03/$ – see front matter © 2003 Elsevier Science B.V. All rights reserved.
doi:10.1016/S0021-9673(02)02084-8

preparative chromatography is carried out at high concentrations, the injected samples often being at concentrations close to those of saturated solutions. Under such conditions, the equilibrium isotherms between the two phases of the chromatographic system are rarely linear. The stronger the nonlinear behavior of the isotherm at the band concentration, the more skewed the band profile, the lower the band resolution, the recovery yield, and the production rate [1]. Mass transfer kinetics affects the precise shape of the band profiles, dispersing the profiles predicted by thermodynamics alone. Accordingly, it has an impact on the band resolution, especially at low column efficiencies [1].

It is thus of the paramount importance to determine the competitive isotherms of the feed components. However, it has been shown that these isotherms can most often be derived from the single component isotherms of these compounds [1,4,5]. Numerous methods are available for the acquisition of equilibrium isotherm data and for the derivation of single-component isotherms. The methods that are the fastest and the most convenient for our purpose are frontal analysis (FA) [1,5–7], elution by characteristic point (ECP) [1,8,9], and pulse methods [1,10,11]. All of these methods have their own advantages and drawbacks which must be taken into account in any specific case, to minimize measurement errors and costs [1]. In this work, we use the FA method, the most accurate but also the slowest.

Most adsorption isotherm models applied in liquid chromatography are semi-empirical extensions of models derived for gas–solid equilibria. The pressure is merely replaced by the eluite concentration in the isotherm equation. A great variety of empirical isotherm models are available to describe the adsorption of eluites in preparative chromatography. Many experimental isotherm data have been fitted to numerous liquid–solid isotherm models [1,5] but it is often observed that the mere agreement between experimental isotherm data and the best isotherm derived from a model of adsorption is not sufficient to describe well the overloaded band profiles. It often turns out that calculated band profiles differ strongly from experimental profiles. This validation test is important. It is not a circular argument because the FA method is independent of the calculation of band profiles.

The theory of liquid–solid adsorption is more complex and less advanced than that of gas–solid equilibria. Important limitations come from the inherent competition for adsorption between the adsorbate and the solvent, which is in large excess, from the multitude of possible interactions between the components of a solution, a situation without equivalent in gas–solid equilibria. A rigorous, quantitative approach to liquid–solid equilibria was elaborated by Everett [12] and Riedo and Kovats [13], based on the consideration of surface excess and excess isotherms. A most serious practical difficulty arises from the heterogeneity of the adsorbent surface used.

This situation is also frequent in gas–solid adsorption where the adsorbent heterogeneity is formally described by use of the adsorption energy distribution (AED). The adsorption behavior on the sites having the same energy is described by an isotherm model valid for a homogeneous surface, the local isotherm model. The two simplest local isotherms with no adsorbate–adsorbate interactions are the Langmuir [14] and the Jovanovic isotherm [15,16] models which need two parameters only, the saturation capacity and the binding energy of the adsorption site. A detailed discussion of gas–solid physical adsorption on heterogeneous surfaces was given by Jaroniec and Madey [17]. This treatment can be extended to liquid–solid equilibria [18]. Unfortunately, the relationship between global adsorption isotherm and AED is given by an integral equation, the solution of which is an ill-posed problem. A variety of methods have been suggested [17–19]. Although all chromatographic surfaces are heterogeneous, the affinity energy distribution [18] has not been used yet to characterized packing material and to investigate their behavior in preparative chromatography.

The goal of this work is to show how the determination of the AED allows a selection of the best isotherm model based on a physically meaningful test and permits a quantitative investigation of the active sites. The direct calculation of the AED from experimental FA data using the expectation maximization (EM) procedure [20,21] gives access to additional physical properties that the isotherm model must fulfill, as illustrated in two examples. Experimental FA data for phenol and caffeine were

acquired on a commercial column, the isotherm data were modeled and the AED calculated from the experimental FA data. The results allow the selection of the best isotherm model.

2. Theory

2.1. Determination of single-component isotherms by frontal analysis

Among the various chromatographic methods available to determine single-component isotherms, frontal analysis (FA) is the most accurate [1–3]. It consists in the step-wise replacement of the stream of mobile phase percolating through the column with streams of solutions of the studied compound of increasing concentrations and in the recording of the breakthrough curves at the column outlet. As previously explained in detail [34], the integral mass balance of the solute between the times when the new solution enters the column and when the plateau concentration is reached allows the calculation of the adsorbed amount, q^*, of solute in the stationary phase at equilibrium at a given mobile phase concentration, C [22]. The adsorbed amount q^* is given by:

$$q^* = \frac{C(V_{eq} - V_0)}{V_a} \quad (1)$$

where V_{eq} and V_0 are the elution volume of the equivalent area and the hold-up volume, respectively, and V_a is the volume of stationary phase.

2.2. Models of single-component isotherm

2.2.1. The Langmuir isotherm

This model is most frequently used in the study of liquid–solid chromatographic equilibria, in spite of its semi-empirical nature [5,9]. It is written:

$$q^* = q_S \cdot \frac{bC}{1 + bC} \quad (2)$$

In this model, q_S is the monolayer saturation capacity of the adsorbent and b is the equilibrium constant of adsorption. This model assumes that the surface of the adsorbent is homogeneous, that the adsorption is localized, and that there are no adsorbate–adsorbate interactions. The equilibrium constant b is given by the following equation [17]:

$$b = b_0 \, e^{\varepsilon_a / RT} \quad (3)$$

where ε_a is the energy of adsorption and b_0 is a preexponential factor that can be derived from the molecular partition functions in both the bulk and the adsorbed phases. In consistence with the basic assumption of this model, the AED function, $F(e)$, of the Langmuir isotherm is a Dirac function:

$$F(\varepsilon) = \delta(\varepsilon - \varepsilon_a) \quad (4)$$

The surface is assumed to be homogeneous and it has a unimodal energy distribution, the width of this mode being 0.

2.2.2. The Bi-Langmuir isotherm

This model is the simplest one for a nonhomogeneous surface [23]. The surface is assumed to be paved with two different types of chemical domains which behave independently. Then, the equilibrium isotherm results from the addition of two independent local Langmuir isotherms:

$$q_S = q_{S,1} \cdot \frac{b_1 C}{1 + b_1 C} + q_{S,2} \cdot \frac{b_2 C}{1 + b_2 C};$$

$$q_S = q_{S,1} + q_{S,2} \quad (5)$$

In this model, there are two saturation capacities, $q_{S,1}$ and $q_{S,2}$, corresponding to each one of the two types of sites. The total saturation capacity of the adsorbent is $q_S = q_{S,1} + q_{S,2}$.The two equilibrium constants b_1 and b_2 are associated with the adsorption energies $\varepsilon_{a,1}$ and $\varepsilon_{a,2}$, through Eq. (3). The AED function becomes:

$$F(\varepsilon) = \frac{q_{S,1}}{q_S} \cdot \delta(\varepsilon - \varepsilon_{a,1}) + \frac{q_{S,2}}{q_S} \cdot \delta(\varepsilon - \varepsilon_{a,2}) \quad (6)$$

This is a bimodal energy distribution and both modes have a width 0.

2.2.3. The Toth isotherm

Toth proposed an empirical isotherm [24,25] to account for the experimental adsorption isotherms that are obtained on nonhomogeneous adsorbents.

$$q^* = q_S \cdot \frac{bC}{[1+(bC)^n]^{1/n}} \quad (7)$$

In this equation, q_S and b have the same meaning as in the Langmuir isotherm model and n is the heterogeneity parameter ($0 < n < 1$). The AED function corresponding to the Toth isotherm model (assuming a local Langmuir isotherm model) is given by the following equation [26]:

$$F(\varepsilon) = \frac{\sin\left[\frac{Y(\varepsilon)}{n}\right]}{\pi RT\left[\left(\frac{y(\varepsilon)}{y(\varepsilon_a)}\right)^{2n} + 2(\cos n\pi)\left(\frac{y(\varepsilon)}{y(\varepsilon_a)}\right)^{n} + 1\right]^{1/2n}} \quad (8)$$

where R is the universal gas constant ($=8.31$ J/mol/K), T is the absolute temperature, $y(\varepsilon)$ and $Y(\varepsilon)$ are two functions of the adsorption energy defined by:

$$y(\varepsilon) = e^{\varepsilon/RT} \quad (9)$$

and

$$Y(\varepsilon) = \arccos \times \left\{ \frac{\cos(n\pi)\left(\frac{y(\varepsilon)}{y(\varepsilon_a)}\right)}{\left[\left(\frac{y(\varepsilon)}{y(\varepsilon_a)}\right)^{2n} + 2(\cos n\pi)\left(\frac{y(\varepsilon)}{y(\varepsilon_a)}\right)^{n} + 1\right]^{1/2n}} \right\} \quad (10)$$

This distribution function is maximum for an adsorption energy equal to ε_a the value of ε which is related to b through Eq. (3). This distribution is asymmetrical and unimodal, it tails toward the low adsorption energies.

2.3. Calculation of the adsorption energy distributions

The experimental isotherm is the sum of the individual contributions of the isotherms of all the homogeneous sites corresponding to an energy of the AED. Under the condition of a continuous distribution and assuming a Langmuir local isotherm model, this sum can be replaced by an integral and the overall adsorption isotherm can be written [17]:

$$q^*(C) = \int_0^\infty F(\varepsilon)\left(\frac{b_0\, e^{\varepsilon/RT}C}{1 + b_0\, e^{\varepsilon/RT}C}\right) d\varepsilon \quad (11)$$

with the normalization condition

$$\int_0^\infty F(\varepsilon)\, d\varepsilon = q_S \quad (12)$$

$q^*(C)$ is the total amount of solute adsorbed on the surface at equilibrium with a concentration C and q_S is the overall saturation capacity.

To investigate the behavior of heterogeneous surfaces, we have to derive $F(\varepsilon)$ from the isotherm data. This can be done using a variety of methods [17,19–21]. Many use a preliminary smoothing of the experimental data and their fit to an isotherm model or search for a AED given by a certain function. We preferred the EM method which uses directly the raw data [21]. The distribution function $F(\varepsilon)$ is discretized using N grid points in the energy space and is estimated from the data points. The energy space is fixed between ε_{min} and ε_{max}. The amount $q(C_i)$ of solute adsorbed at concentration C_j is iteratively estimated by:

$$q^k_{cal}(C_j) = \sum_{\varepsilon_{min}}^{\varepsilon_{max}} F^k(\varepsilon_i) \cdot \frac{b_0\, e^{\varepsilon_i/RT}C_j}{1 + b_0\, e^{\varepsilon_i/RT}C_j} \cdot \Delta\varepsilon \quad j \in [1,M]; i \in [1,N] \quad (13)$$

with

$$\Delta\varepsilon = \frac{\varepsilon_{max} - \varepsilon_{min}}{N-1} \quad \varepsilon_i = \varepsilon_{min} + (i-1)\,\Delta\varepsilon \quad (14)$$

The index k states for the kth iteration of calculation of the AED function. The initial guess (iteration $k=0$) of the AED function $F(\varepsilon_i)$ is the uniform distribution of the maximum adsorbed amount observed experimentally, over the N fictitious adsorption sites. It has the advantage of introducing a minimum of bias into the calculation of the AED:

$$F^0(\varepsilon_i) = \frac{q(C_M)}{N} \quad \forall i \in [1,N] \quad (15)$$

Actually, the EM program calculates the amount adsorbed by taking $b(\varepsilon_i)$ as the variable of the energy space, so that neither temperature nor preexponential factor need to be defined. Only M, N, b_{min}, b_{max} and the number of iterations must be defined to start the

calculation. It is noteworthy that, to obtain any information on the adsorption energy, an assumption must be made for b_0. The final result is a distribution of equilibrium constants.

The distribution function is updated at the kth iteration by:

$$F^{k+1}(\varepsilon_i) = F^k(\varepsilon_i) \sum_{\varepsilon_{\min}}^{\varepsilon_{\max}} \frac{b_0 \, e^{\varepsilon_i/RT} C_j}{1 + b_0 \, e^{\varepsilon_i/RT} C_j} \cdot \Delta\varepsilon \frac{q_{\exp}(C_j)}{q^k_{\text{cal}}(C_j)} \tag{16}$$

The EM procedure protects better than most other methods against the consequences of possible experimental artifacts which can be incorporated in the calculation of AED or against the effect of modeling the experimental data or the AED.

2.4. Modeling of high-performance liquid chromatography

The profiles of overloaded bands were calculated using the equilibrium-dispersive (ED) model of chromatography [1,5,27]. This model assumes instantaneous equilibrium between the mobile and the stationary phases and a finite column efficiency. The latter is assumed to originate from an apparent axial dispersion coefficient, D_a, accounting for all the dispersive phenomena (molecular and eddy diffusion and non-equilibrium effects) that take place in a chromatographic column. The axial dispersion coefficient is:

$$D_a = \frac{uL}{2N} \tag{17}$$

where u is the mobile phase linear velocity, L the column length, and N the number of theoretical plates or apparent efficiency of the column.

In this model, the mass balance equation for a single component is expressed as follows:

$$\frac{\partial C}{\partial t} + u \cdot \frac{\partial C}{\partial z} + F \cdot \frac{\partial q^*}{\partial t} - D_a \cdot \frac{\partial^2 C}{\partial z^2} = 0 \tag{18}$$

where q^* and C are the stationary and mobile phase concentrations of the adsorbate, respectively, t is the time, z the distance along the column and $F = (1 - \varepsilon)/\varepsilon$ is the column phase ratio. q^* is related to C through the isotherm equation, $q^* = f(C)$. ε is the total column porosity.

2.4.1. Initial and boundary conditions for ED model

At $t = 0$ the concentration of the adsorbate in the column is uniformly equal to zero and the stationary phase is in equilibrium with the pure mobile phase. The boundary conditions used are the classical Dankwerts-type boundary conditions [28] at the inlet and outlet of the column.

2.4.2. Numerical solutions of the ED model

The ED model was solved using a computer program based on an implementation of the method of orthogonal collocation on finite elements [29–31]. The set of discretized ordinary differential equations was solved with the Adams–Moulton method, implemented in the VODE procedure [32]. The relative and absolute errors of the numerical calculations were 1×10^{-6} and 1×10^{-8}, respectively.

3. Experimental

3.1. Chemicals

The mobile phase used in this work, whether for the determination of the adsorption isotherms data of for the recording of large size band profiles was a mixture of HPLC-grade water and methanol [methanol–water (30:70, v/v) for caffeine and methanol–water (45:55, v/v) for phenol], both purchased from Fisher Scientific (Fair Lawn, NJ, USA). The solvents used to prepare the mobile phase were filtered before use on an SFCA filter membrane, 0.2 μm pore size (Suwannee, GA, USA). Uracil, caffeine and phenol were obtained from Aldrich (Milwaukee, WI, USA).

3.2. Materials

A manufacturer-packed Kromasil-C_{18}, 250×4.6 mm, column was used. This C_{18}-bonded, endcapped packed column (column E6019, Eka, Bohus, Sweden) was one of the lot of 10 columns previously used by Kele and Guiochon [33] (column E6019, E6103–E6106, E6021–E6024 and E6436) for their study of the reproducibility of the properties of RPLC columns under linear conditions. The main characteristics of the bare silica and of the packing material used are summarized in Table 1.

Table 1
Physicochemical properties of the packed Kromasil-C_{18} (Eka) #E6019 column

Particle size	5.98 μm
Particle size distribution (90:10, % ratio)	1.44
Pore size	112 Å
Pore volume	0.88 cm^3/g
Surface area	314 m^2/g
Na, Al, Fe content	11; <10; <10 ppm
Particle shape	Spherical
Total carbon	20.00%
Surface coverage	3.59 $\mu mol/m^2$
Endcapping	Yes

The hold-up time of this column was determined from the retention time of uracil injections. For mobile phase compositions in the range (30:70, v/v) to (45:55, v/v), the elution time of uracil is nearly the same as that of methanol or sodium nitrate. It permits the determination of an excellent estimate of the column void volume. The dead volumes of the column (and the total porosity ε_t) in methanol–water (30:70, v/v) and (45:55, v/v) mobile phases are 2.63 and 2.46 cm^3, respectively.

3.3. Apparatus

The data were acquired using a Hewlett-Packard (Palo Alto; CA, USA) HP 1090 liquid chromatograph. This instrument includes a multi-solvent delivery system (tank volume, 1 dm^3 each), an auto-sampler with a 25-mm^3 loop, a diode-array UV detector, a column thermostat and a computer data acquisition station. Compressed nitrogen and helium bottles (National Welders, Charlotte, NC, USA) are connected to the instrument to allow the continuous operation of the pump and auto-sampler. The extra-column volumes are 0.068 and 0.90 cm^3 as measured from the auto-sampler and the pump system, respectively, to the column inlet. All the retention data were corrected for this contribution. All measurements were carried out at a constant temperature of 23 °C.

3.4. Frontal analysis isotherm measurements

The mobile phase composition at which the FA measurements were performed was chosen depending on the retention factor of the solutes at infinite dilutions. In order to be able to acquire a sufficient number of data points and to achieve measurements of a satisfactory accuracy, the retention factor should be neither too high nor too low. Values between 2 and 3 are ideal. Prior to any isotherm determination, the solubilities at 23 °C of phenol and caffeine were determined approximately by the stepwise additions of 5 ml of the pure mobile phase into a volume of 250 cm^3 of a saturated solution until complete dissolution. Accordingly, the maximum concentrations used in FA measurements were 30 and 34 g/dm^3 for phenol and caffeine, respectively (in the corresponding mobile phase). Two master sample solutions were prepared, with concentrations of 15 and 100% of these maximum concentrations, respectively. Two consecutive series of FA measurements were carried out with these solutions, covering a wide range of concentrations. Thirty-five experimental adsorption data points were recorded for each compound.

One pump of the HPLC instrument was used to deliver a stream of the pure mobile phase, the second pump a stream of pure sample solution. The concentration of the studied compound is determined by the concentration of the mother sample solution and the flow-rate fractions delivered by the two pumps. The breakthrough curves are recorded successively at a flow-rate of 1 cm^3 min, with a sufficiently long time delay between each breakthrough curve to allow for the reequilibration of the column with the pure mobile phase. The injection time of the sample was fixed at 5 min in order to reach a stable plateau at the column outlet. The signals of phenol and caffeine were detected with the UV detector at 290 and 308 nm, respectively.

The overloaded profiles needed for the validation of the fitted isotherms were recorded when the frontal analysis experiments were done.

4. Results and discussion

4.1. Fitting models for the experimental single isotherms of phenol and caffeine

Figs. 1 and 2 show the adsorption data (symbols)

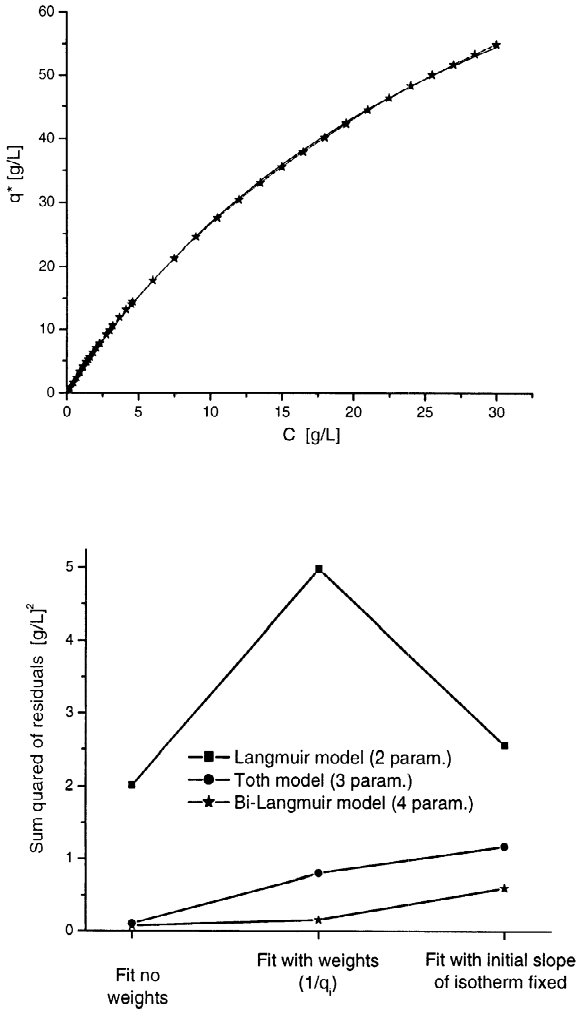

Fig. 1. Experimental isotherm of phenol on the packed Kromasil-C_{18} column with methanol–water (45:55, v/v) as the mobile phase. The solid, the dash-dotted and the dotted lines are the best fitting isotherms using a Langmuir, Toth and Bi-Langmuir models, respectively. $T=295$ K. Note the equivalency of the three models regarding the fit of the experimental data. The bottom graph represents the evolution of the residuals of the isotherm fittings, illustrating the trend of the fitting errors.

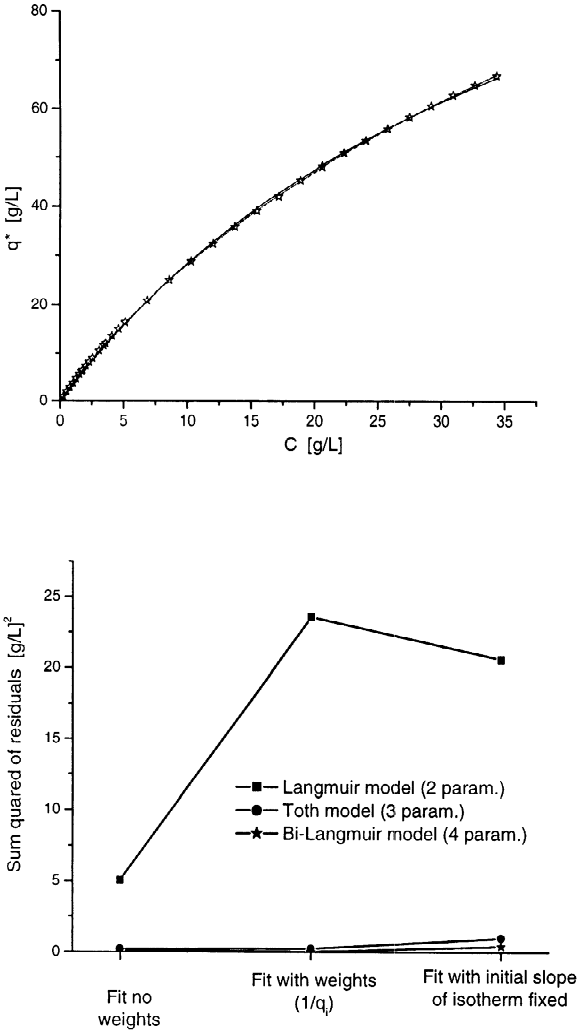

Fig. 2. Experimental isotherm of caffeine on the packed Kromasil-C_{18} column with methanol–water (30:70, v/v) as the mobile phase. The solid, the dash-dotted and the dotted lines are the best fitting isotherms using a Langmuir, Toth and Bi-Langmuir models, respectively. $T=295$ K. Note again the equivalency of the three models regarding the fit of the experimental data. The bottom graph represents the evolution of the residuals of the isotherm fittings, illustrating the trend of the fitting errors.

for phenol and caffeine, respectively, derived from the FA measurements at 23 °C. Both isotherms are convex upward. The breakthrough curves exhibit a characteristic front shock while the breakthrough of the mobile phase when the column is regenerated has a dispersive profile. The experimental data fit well to three different models of adsorption isotherms,

1. The Langmuir model with two parameters (q_S and b).
2. The Toth model with three parameters (q_S, b and n).
3. The Bi-Langmuir model with four parameters ($q_{S,1}$, b_1, $q_{S,2}$, and b_2).

The lines in Figs. 1 and 2 show the best isotherms

obtained for the two compounds. These lines are very close to the 35 experimental data points. The curves for the Langmuir, the Toth and the Bi-Langmuir isotherms (solid, short- and long-dotted lines, respectively) are impossible to distinguish at the scale of the figure. The small differences between these curves illustrate the figures of statistical merit calculated for these isotherms (Table 2).

Table 2 summarizes the results of the nonlinear regression of the experimental FA data on the three models. The higher the number of parameters in the model, the higher the statistical test values for both compounds. All the numerical values of the parameters obtained make physical sense and their magnitude is acceptable. We showed previously [34] that the total saturation capacity q_S of compounds with small molecules on the C_{18} bonded silica used as packing material for RPLC is usually of the order of a few hundreds grams per liter and their equilibrium constant b is about a few hundredths of a liter per gram. The values reported in Table 2 are within these ranges. We also know that the heterogeneity parameter n is always less than 1, as it is here for both compounds. The Fisher test value is about 20 and 30 times less for the Langmuir model than for the Toth and the Bi-Langmuir models, respectively. This statistically shows a significant difference between the Langmuir model and the other two models. By contrast, we cannot say, at a confidence level of 5%, which one of the Toth and the Bi-Langmuir models accounts better for the experimental data since the ratio of their respective Fisher test values is less than the required 2.0.

In conclusion, it is difficult at this stage to ascertain the physical meaning of the results of this statistical exercise. The three isotherm models seem to account very well for the experimental results. However, they need to be subjected to a validation test concerning their ability to predict the elution profiles of overloaded chromatographic bands.

4.2. Comparison between experimental and calculated band profiles

In order to check the validity of isotherm models, they are combined with a proper dynamic model of chromatography and used to calculate the elution profiles of high concentration breakthrough curves and of large-size bands. The calculated profiles are then compared with experimental results. Band profiles of phenol and caffeine were calculated with each of the three models selected and the results compared to experimental profiles obtained under different loading conditions. The calculations were performed using the ED model. This model is sufficiently sophisticated to model the band profiles of compounds with small molecules for which mass transfer kinetics is fast and a more complex model is not necessary.

4.2.1. Linear conditions

First the profiles calculated with the three models under infinite dilution are considered and compared to experimental peaks obtained with 2-μg samples (2 ml of a 1 g/dm^3 solution). The retention time of these pulses is related to the initial slope of the

Table 2
Adsorption isotherm fitting of phenol methanol–water (45/55, v/v) and caffeine methanol–water (30/70, v/v) on Kromasil-C_{18} column

Langmuir	Fisher	q_S	IC_{95} (%)	b	IC_{95} (%)				
Phenol	5 585	111.9	1.9	0.03140	3.0				
Caffeine	3 258	146.5	2.8	0.0239	4.2				
Toth	Fisher	q_S	IC_{95} (%)	b	IC_{95} (%)	n	IC_{95} (%)		
Phenol	106 000	161.5	3.9	0.02414	2.9	0.7610	2.4		
Caffeine	69 910	280.9	7.0	0.01459	5.6	0.6586	3.6		
Bi-Langmuir	Fisher	$q_{S,1}$	IC_{95} (%)	b_1	IC_{95} (%)	$q_{S,2}$	IC_{95} (%)	b_2	IC_{95} (%)
Phenol	147 600	121.4	2.0	0.01743	24.1	17.72	6.2	0.09306	31.9
Caffeine	136 100	168.9	1.8	0.01692	5.9	05.18	31.6	0.2305	28.4

Fisher test values, best isotherm parameters and their associated 95% confidence interval obtained by regression analysis on three models (Langmuir, Toth and Bi-Langmuir).

isotherm (also called the Henry constant H) and to the column phase ratio F. Conversely, from the retention time measured, one can derive H.

$$t_R = t_0(1 + FH): \; F = \frac{1 - \varepsilon_t}{\varepsilon_t} \tag{19}$$

Table 3 lists the Henry constants found for each fitting model and those derived from the retention time of analytical injection and the initial linear part of the FA data. The agreement between the first frontal analysis data (linear fitting of the first five data points, corresponding to concentrations between 0 and 1 g/dm^3) and the data derived from the retention times of impulses is very close for both compounds (see Figs. 3 and 4). The differences between the retention times of the experimental pulses and those calculated from the initial slope of the experimental isotherm are only 0.16 and 0.03% for phenol and caffeine, respectively. This result confirms that the measurements of the extra-column volumes (0.068 and 0.900 cm^3 from the syringe and the pump delivery system) were correct and that

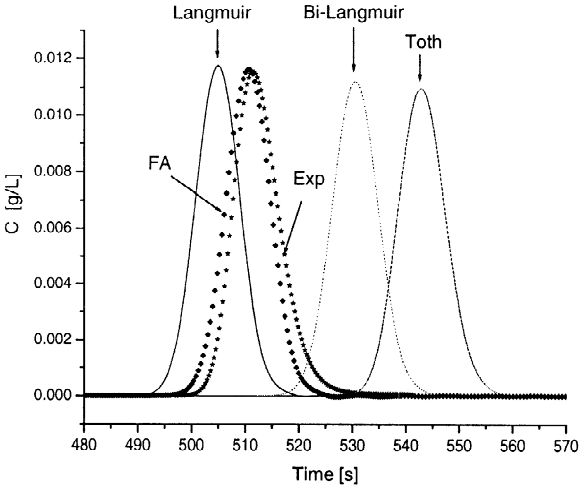

Fig. 3. Injection of 2 ml of a solution of phenol at 1 g/dm^3 on the packed Kromasil-C_{18} column with methanol–water (45:55, v/v) as the mobile phase. Comparison between simulated profiles (using the Henry constant of each model and a linear isotherm) and the experimental profile. The profile located by FA is a simulated profile using a linear isotherm whose slope is determined by the five first FA data points in the range [0;1] g/dm^3. Note the perfect agreement between this profile and the experimental one. $T = 295$ K.

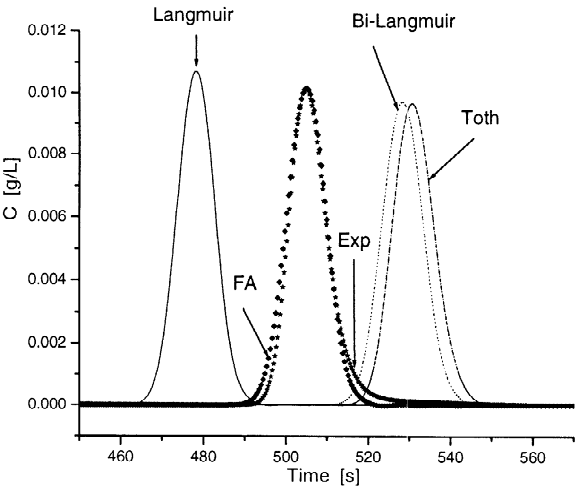

Fig. 4. Injection of 2 ml of a solution of caffeine at 1 g/dm^3 on the packed Kromasil-C_{18} column with methanol–water (30:70, v/v) as the mobile phase. Comparison between simulated profiles (using the Henry constant of each model and a linear isotherm) and the experimental profile. The profile located by FA is a simulated profile using a linear isotherm whose slope is determined by the five first FA data points in the range [0;1] g/dm^3. Note again the perfect agreement between this profile and the experimental one. $T = 295$ K.

these corrections are properly accounted for in the calculation of the amount adsorbed in the stationary phase.

It turned out, however, that the isotherm model obtained from the fitting of the data acquired in the whole range of concentrations (0 to 30 and 0 to 34 g/dm^3) does not afford an exact prediction of the pulse retention time. The error is approximately 1.2% with the Langmuir isotherm, 4% with the Bi-Langmuir isotherm, and 6.5% with the Toth isotherm. The main reason for the error made is that all the data points were weighed uniformly ($\omega_i = 1/N$) in the classical regression analysis made. The influence of the high concentration data points on the values obtained for the numerical coefficients is higher than that of the low concentration data points. To account better for the low concentration behavior of the isotherm, it is possible to weigh the data points in the regression by the factor $\omega_i = 1/q_i^2$.

In this case (with results in Table 3), the initial slopes of the Langmuir, Toth and Bi-Langmuir isotherm models become closer to the correct one for phenol (see Table 3). For caffeine, however, the

Table 3

Compound	t_0 (min)	ε_t	F	H_{exp}	H_{FA}	$H_{Langmuir}$	H_{Toth}	$H_{Bi\text{-}Langmuir}$
Phenol	2.458	0.5916	0.6896	3.578	3.568	3.514	3.899	3.765
caffeine	2.628	0.6325	0.5809	3.791	3.792	3.501	4.098	4.052

parameters of the Toth and the Bi-Langmuir models are not significantly affected. Conversely, the Henry constant is in much better agreement with the experimental data in the case of the Langmuir model.

4.2.2. Validity of the models from low to high concentrations

We proposed now to check the validity of the models in the whole range of concentration investigated in the FA experiments. For that purpose, we recalculated the best isotherm parameters by adding a new constraint, forcing the value of the Henry constant to be equal to the value measured at infinite dilution. The constraints imposed to the model parameters are thus:

$$q_S b = q_{S,1} b_1 + q_{S,2} b_2 = 3.758 \text{ for phenol}$$
$$q_S b = q_{S,1} b_1 + q_{S,2} b_2 = 3.791 \text{ for caffeine}$$

As expected, the Fisher number decreases with the introduction of this new constraint on the model parameters but the results obtained with the two compounds and the three models are quite different (Table 4). The Fisher number for phenol is divided by a mere factor 1.3 for the Langmuir model and 10-fold for the Toth and the Bi-Langmuir isotherms. Furthermore, the Bi-Langmuir parameters have no longer any physical sense. Conversely, the Fisher number for caffeine is divided by a factor of approximately 4 for all three isotherm models. However, the parameters of all the isotherm models still have values consistent with their physical meaning.

In other words, the Langmuir model gives the best account of the experimental isotherm of phenol at low and high concentrations. This is not true for the Toth or the Bi-Langmuir model, neither of which can account properly for the isotherm behavior at low and at high concentrations at the same time. By contrast, these last two isotherm models account well for the behavior of the isotherm of caffeine in the whole concentration range investigated while the Langmuir model fails to account for this behavior at all concentrations.

This conclusion is explained in part by the experimental plot of q^*/C versus q^* (i.e., the Scatchard plot, Figs. 5 and 6). The Scatchard plot of a Langmuir isotherm is a straight line. For a Bi-Langmuir isotherm, it is a convex downward curve with no inflection point, that has two asymptotes, one at low, one at high concentrations, both with a negative slope proportional to the binding energy of

Table 4
Adsorption isotherm fitting of phenol methanol–water (45/55, v/v) and caffeine methanol–water (30/70, v/v) on Kromasil-C_{18} column using the true Henry constant as a physical constraint

Langmuir	Fisher	q_S	IC_{95} (%)	b	IC_{95} (%)				
Phenol	4 508	109.1	0.8	0.03279	0.8				
Caffeine	825	130.0	1.9	0.02916	1.9				
Toth	Fisher	q_S	IC_{95} (%)	b	IC_{95} (%)	n	IC_{95} (%)		
Phenol	9 560	124.4	4.6	0.02877	4.6	0.9258	2.5		
Caffeine	16 240	209.1	4.8	0.01813	4.8	0.7823	2.0		
Bi-Langmuir	Fisher	$q_{S,1}$	IC_{95} (%)	b_1	IC_{95} (%)	$q_{S,2}$	IC_{95} (%)	b_2	IC_{95} (%)
Phenol	16 620	8355	637.1	0.000043	640.0	80.6	54.7	0.03993	26.0
Caffeine	38 330	176.3	7.2	0.01223	27.8	19.7	5.3	0.08314	25.4

Fisher test values, best isotherm parameters and their associated 95% confidence interval obtained by regression analysis on three models (Langmuir, Toth and Bi-Langmuir).

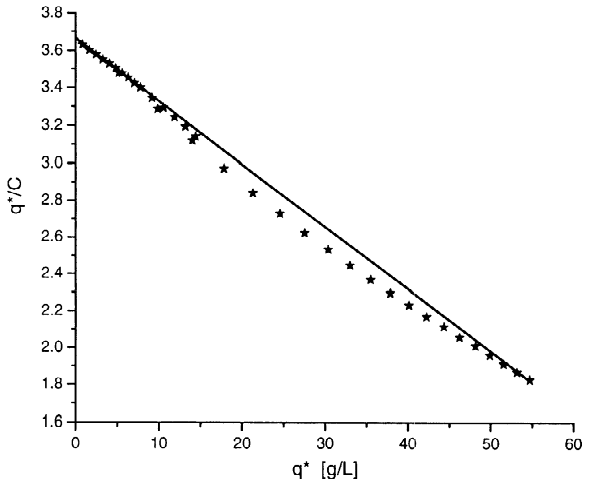

Fig. 5. Scatchard plot (q^*/C as a function of q^*) of phenol on the packed Kromasil-C_{18} column with methanol–water (45:55, v/v) as the mobile phase. Note the close to linearity experimental curve. The solid line is the reference for a pure Langmuir isotherm and allows to show the slight convex upward shape of the plot.

the corresponding sites. For a Toth isotherm, the Scatchard plot is a convex downward curve in the whole concentration range, with a convexity that increases with decreasing heterogeneity parameter.

Fig. 5 clearly shows that the Scatchard plot of phenol is a straight line up to 10 g/dm^3. Then, it slightly deviates from linear behavior, becomes convex downward, passes through two inflection points, and return almost to the extension of the initial straight line at concentrations above 50 g/dm^3. This unusual behavior explains the failure of the Toth and the Bi-Langmuir isotherm models when the initial slope of the isotherm is fixed. As a consequence, it will be difficult accurately to describe the chromatographic behavior of large samples of phenol with a single isotherm model in the full range of concentration.

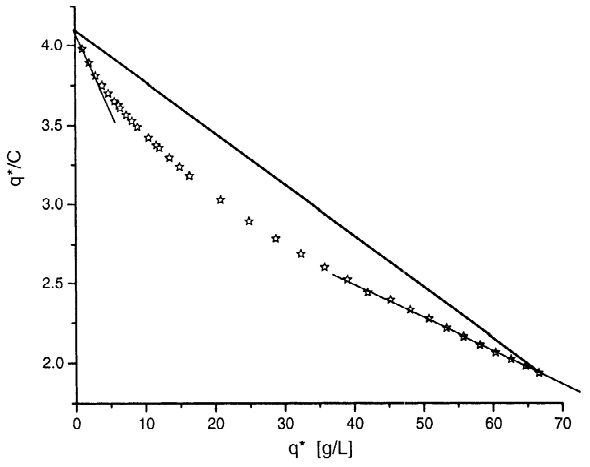

Fig. 6. Scatchard plot (q^*/C as a function of q^*) of caffeine on the packed Kromasil-C_{18} column with methanol–water (30/70, v/v) as the mobile phase. Note, by comparison to Fig. 5, the larger distance between the plot and the hypothetical Langmuir straight line.

Conversely the Scatchard plot of caffeine, like that of compounds exhibiting Bi-Langmuir isotherm behavior, is convex donwnward in the whole concentration range (Fig. 6). In this case, the Bi-Langmuir and the Toth isotherm account well for the experimental data in the whole concentration range. The Langmuir model cannot give satisfactory results.

4.2.3. Simulation of overloaded peaks under non-linear conditions

We compared to the experimental elution profiles the band profiles calculated with the three isotherm models (from Table 2) derived from the experimental isotherm data. Such a comparison requires some caution. Axial dispersion of the solute takes place in the extra-column volume (0.9 cm^3) of the HPLC instrument to a significant degree. The inlet profiles were recorded by connecting directly the detector to the injection device and adding a short length (ca 10 cm) of a 0.0025 inch tubing to allow the pump to operate against a significant hydraulic resistance (1 in = 2.54 cm). The inlet profiles obtained are shown in Fig. 7. They are very different from those applied to the pilot of the pump delivery system. The front and rear parts are markedly dispersed. For the largest sample, it takes 40 s for the inlet concentration to raise from 0 g/dm^3 to the maximum concentration, a behavior quite different from the expected concentration shock. These inlet profiles were used as the boundary conditions in the calculation program, instead of the rectangular profiles used in theoretical studies. An accurate modeling of the rear part of the inlet profile is required for the correct calculation of band profiles obtained with convex upward isotherms. Since the propagation velocity associated with a concentration increases with increasing concentration, the dispersion due to the tailing of the

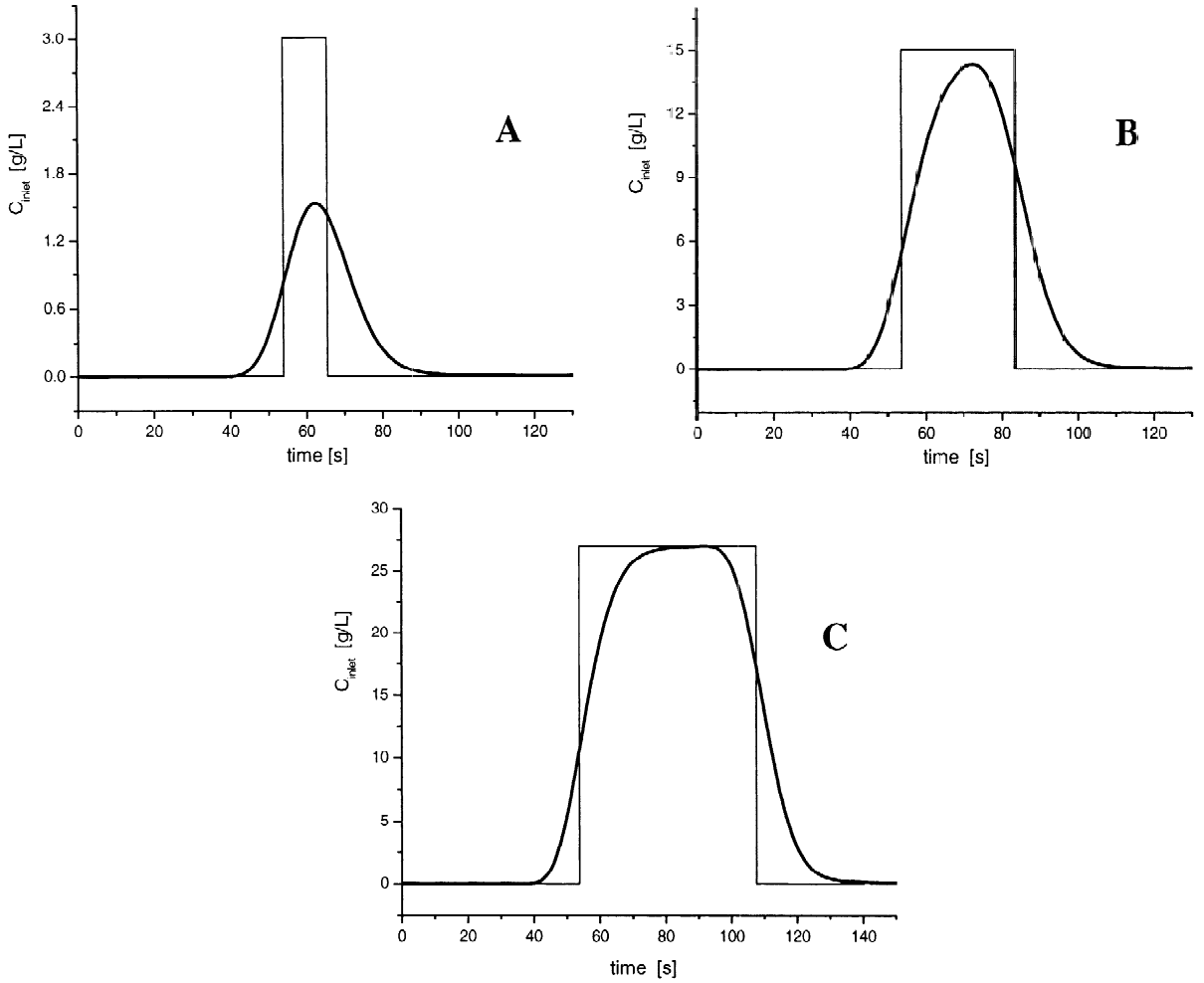

Fig. 7. Comparison between the experimental (thick line) and ideal (thin line) inlet column profiles. (A) Injection of a solution of phenol at 3 g/dm^3 during 12 s. (B) Injection of a solution of phenol at 15 g/dm^3 during 30 s. (C) Injection of a solution of phenol at 27 g/dm^3 during 54 s. Flow rate 1 cm^3/min, T=295 K. Note the large difference of mass distributions (especially for the lowest column loadings) which are highly smoothed.

inlet signal will enhance the spreading of the rear of the profile. The dispersive effect of the fronting of the inlet profile is mitigated by the self-sharpening of the band front. The converse is true for convex downward isotherms.

Three sample sizes, corresponding to loading factors of approximately 0.3, 3 and 10% for each compound, were recorded. The calculated and experimental profiles are shown in Figs. 8 and 9 for phenol and caffeine, respectively. As suggested by the results discussed in the previous section, the agreement between calculated and experimental profiles is only fair at the lowest loading factor (L_f= 0.3%, Figs. 8a and 9a), although the profiles derived from the Toth or the Bi-Langmuir models, corrected for the difference in retention times, would overlay reasonably well to the experimental ones. Despite a better agreement on the retention time, the profile derived from the Langmuir model does not agree well with the experimental one because it is too squat.

The profiles derived from the Langmuir model remain unsatisfactory at higher loading factors (L_f= 3 and 10%, Figs. 8b,c and 9b,c, respectively). The

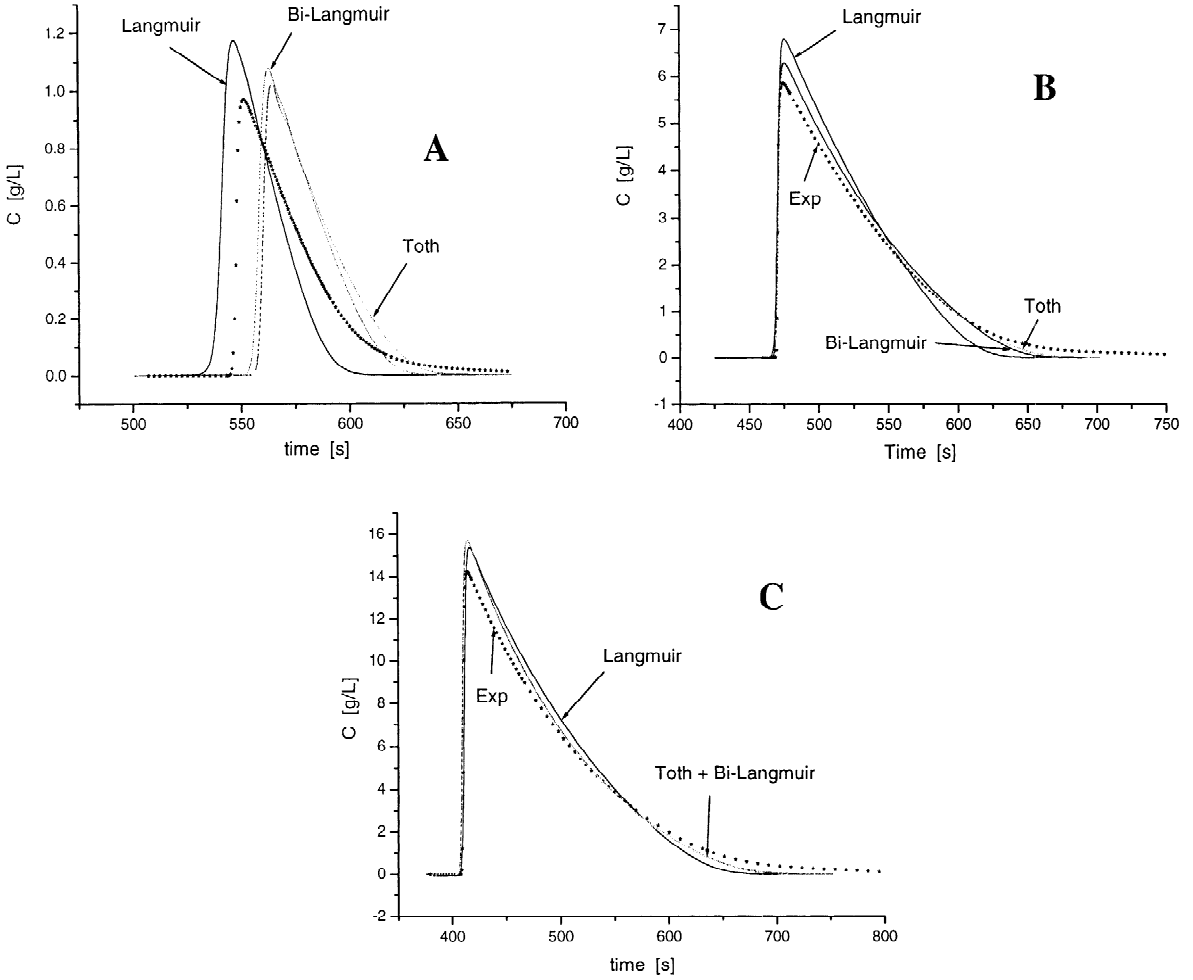

Fig. 8. Comparison between calculated (solid line, Langmuir model; dash-dotted line, Toth model; dotted line, Bi-Langmuir model) and experimental (stars plot) band profiles of phenol on the packed Kromasil-C_{18} column with methanol–water (45:55, v/v) as the mobile phase. (A) Injection of a solution of phenol at 3 g/dm^3 during 12 s. $L_f \approx 0.3\%$. (B) Injection of a solution of phenol at 15 g/dm^3 during 30 s. $L_f \approx 3\%$. (C) Injection of a solution of phenol at 27 g/dm^3 during 54 s. $L_f \approx 10\%$. Flow rate 1 cm^3/min, $T = 295$ K.

rear parts of the calculated bands are systematically steeper than the experimental ones. Conversely, the experimental profiles are well accounted for by those calculated with the Toth and the Bi-Langmuir isotherms which model very well the band tail. These bands remain too high in the case of phenol, however, while the agreement is excellent for caffeine.

As a consequence, the Langmuir model is proven to be unacceptable to account for the behavior of either compound on the stationary phase. It is surprising, however, to observe that two models as different as the Bi-Langmuir and the Toth models generate so similar band profiles. It is, therefore, important that the investigation of the affinity energy distribution calculated directly from the experimental data can give critical clues regarding the best isotherm model.

4.3. Determination of the AED of the experimental adsorption data

The surfaces of actual adsorbents are not homogeneous. Instead, there is a distribution of adsorption

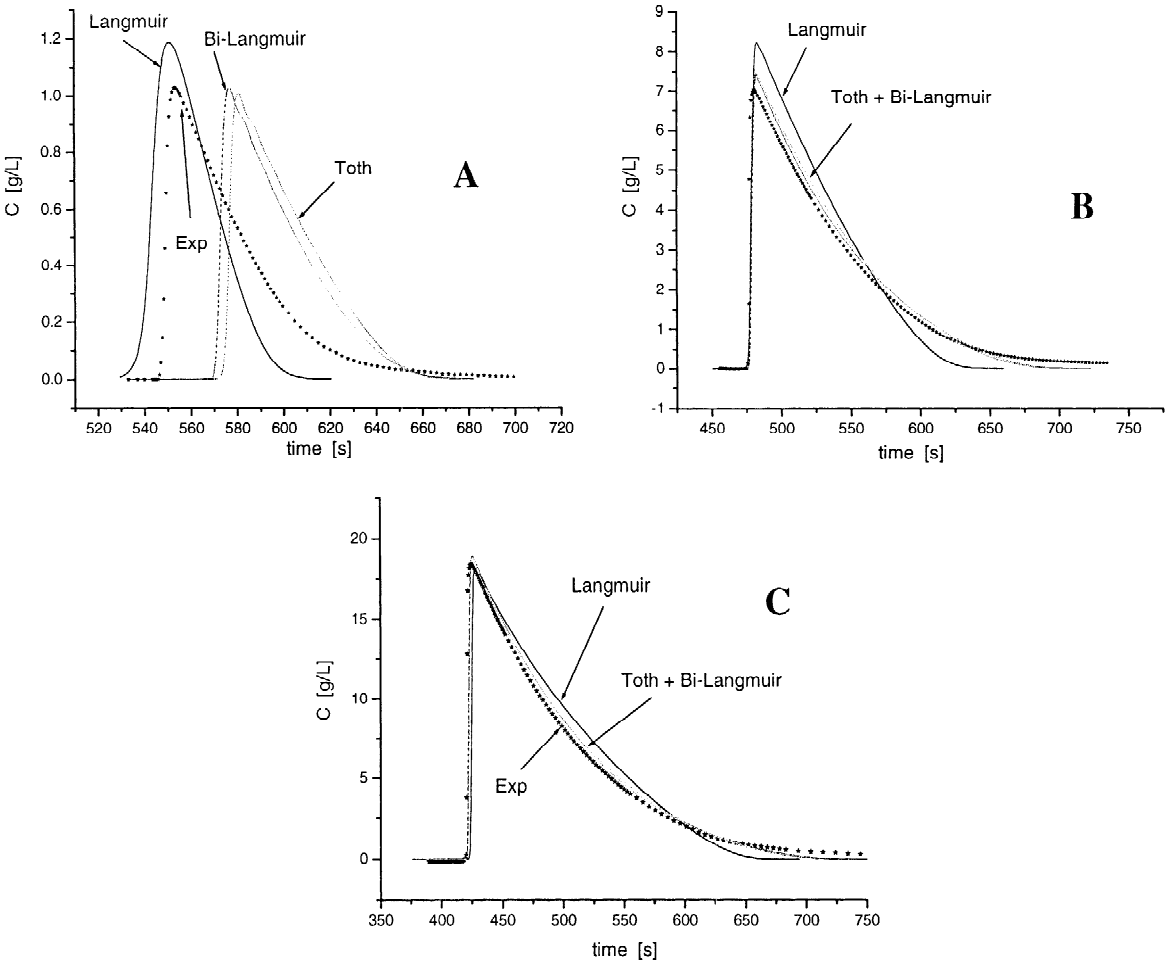

Fig. 9. Comparison between calculated (solid line, Langmuir model; dash-dotted line, Toth model; dotted line, Bi-Langmuir model) and experimental (stars plot) band profiles of caffeine on the packed Kromasil-C_{18} column with methanol–water (30:70, v/v) as the mobile phase. (A) Injection of a solution of caffeine at 3.4 g/dm^3 during 12 s. $L_f \approx 0.3\%$. (B) Injection of a solution of phenol at 17 g/dm^3 during 30 s. $L_f \approx 3\%$. (C) Injection of a solution of phenol at 30.6 g/dm^3 during 54 s. $L_f \approx 10\%$. Flow rate 1 cm^3/min, $T = 295$ K.

energies with a finite width [17]. To each experimental adsorption isotherm, is associated an adsorption energy distribution (see Section 2). Although this concept originates from gas–solid adsorption studies, it is readily extended to liquid–solid adsorption [18]. Accordingly, the important physical difference between the Toth and the Bi-Langmuir isotherms is that the former is characterized by an asymmetric unimodal energy distribution (see Eqs. (8)–(10)) whereas the latter is characterized by a discrete distribution of two distinct energies given by Eq. (6). There are two general approaches used to derive affinity distributions. The former consists in deriving it from the best isotherm model that can be fitted to the adsorption isotherm data. The second consists in a direct calculation of the solution of the Fredholm integral equation (Eq. (11)) that relates the experimental isotherm, the local isotherm, and the affinity energy distribution. Obviously, for our present purpose a method belonging to the second group is needed. These methods use the raw adsorption data and make no assumptions regarding the functional form of the isotherm.

Stanley and Guiochon [21] developed a method

that allows the calculation of the AED of a surface for a given probe from the adsorption isotherm data in gas [35–37] or liquid chromatography [16,38]. This method is based on an expectation maximization (EM) algorithm [20], is iterative and robust. It permitted the analysis of the surface heterogeneity of various silicas and the investigation of the band tailing of strongly basic compounds in RP-HPLC [38]. We used this method to compare the physical meaning of the isotherms considered earlier.

4.3.1. Case of phenol

Fig. 10A shows four successive stages of the calculation of the AED functions of phenol, obtained with the 36 experimental data points. These four stages correspond to increasing numbers of iterations applied in the algorithm (the main drawback of the method is its slow rate of convergence). As the number of iterations increases, a bimodal energy distribution becomes obvious. The integrals of the two modes correspond to their saturation capacities and are 127.9 and 38.9 g/dm^3 for $q_{S,1}$ (low energy sites) and $q_{S,2}$ (high energy sites), respectively. These values are close to those derived from the best fit of the isotherm data to the Bi-Langmuir isotherm model. The theoretical affinity distribution for this isotherm is given in Fig. 10B, with saturation capacities of 121.4 and 17.7 g/dm^3 (see Table 2). The corresponding adsorption energies (energies corresponding to the maximum of each mode of the distribution) are 0.00993 and 0.06338 g/dm^3, to be compared to the values derived from the isotherm model, 0.01743 and 0.09306 g/dm^3. It is noteworthy that the two energies derived from the calculation of the affinity distribution are equal to those derived from the isotherm fit, shifted to lower energies by approximately half a logarithmic unit. The affinity energy distribution obtained differs markedly from the theoretical distribution of the Toth model (Fig. 11C), for which a unimodal energy distribution is observed. This result suggests that the Bi-Langmuir isotherm makes far better physical sense as a model for the adsorption behavior of phenol on the stationary phase studied.

Before proceeding further, we checked the consistency of these results to ascertain that the convergence toward the AED in Fig. 10 was not a chance event. For that purpose, we simulated the determination of an AED. Using successively the Bi-Langmuir and the Toth models with the parameters in Table 2, we calculated a regularly spaced series of adsorption data points and rounded them off with the same precision as that of the experimental data. This introduces a small amount of noise. These data are then used to calculate the corresponding AEDs with the EM method. The results of this exercise are

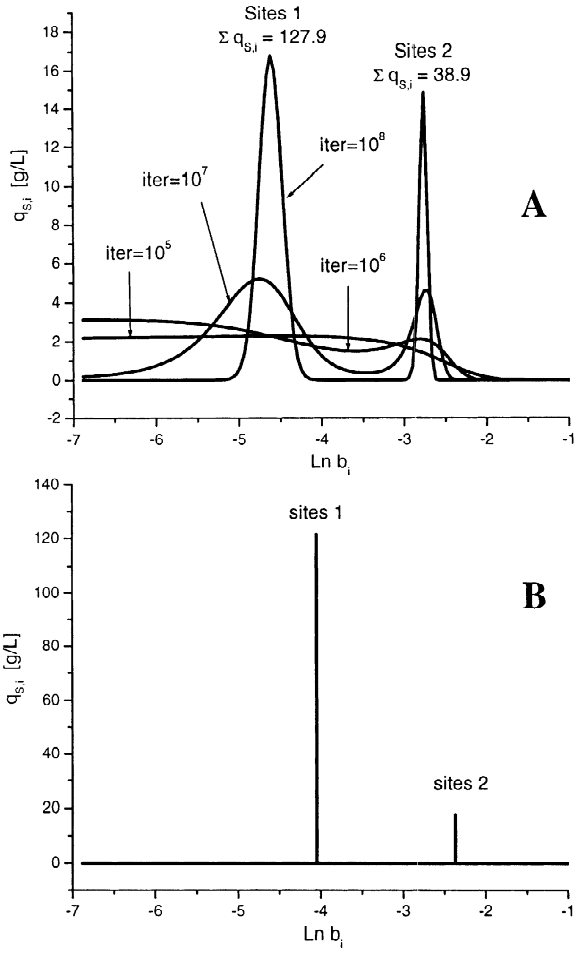

Fig. 10. Adsorption energy distribution (AED) of phenol on the packed Kromasil-C_{18} column with methanol–water (45:55, v/v) as the mobile phase. (A) AED calculated from 36 experimental adsorption data points using the EM program (the values of q^* are truncated at the fifth decimal). The energy space is divided into 150 points. Four different numbers of iteration are used as indicated on the graph. (B) Theoretical AED of the best Bi-Langmuir isotherm found by regression analysis of the same 36 adsorption data points. $T = 295$ K.

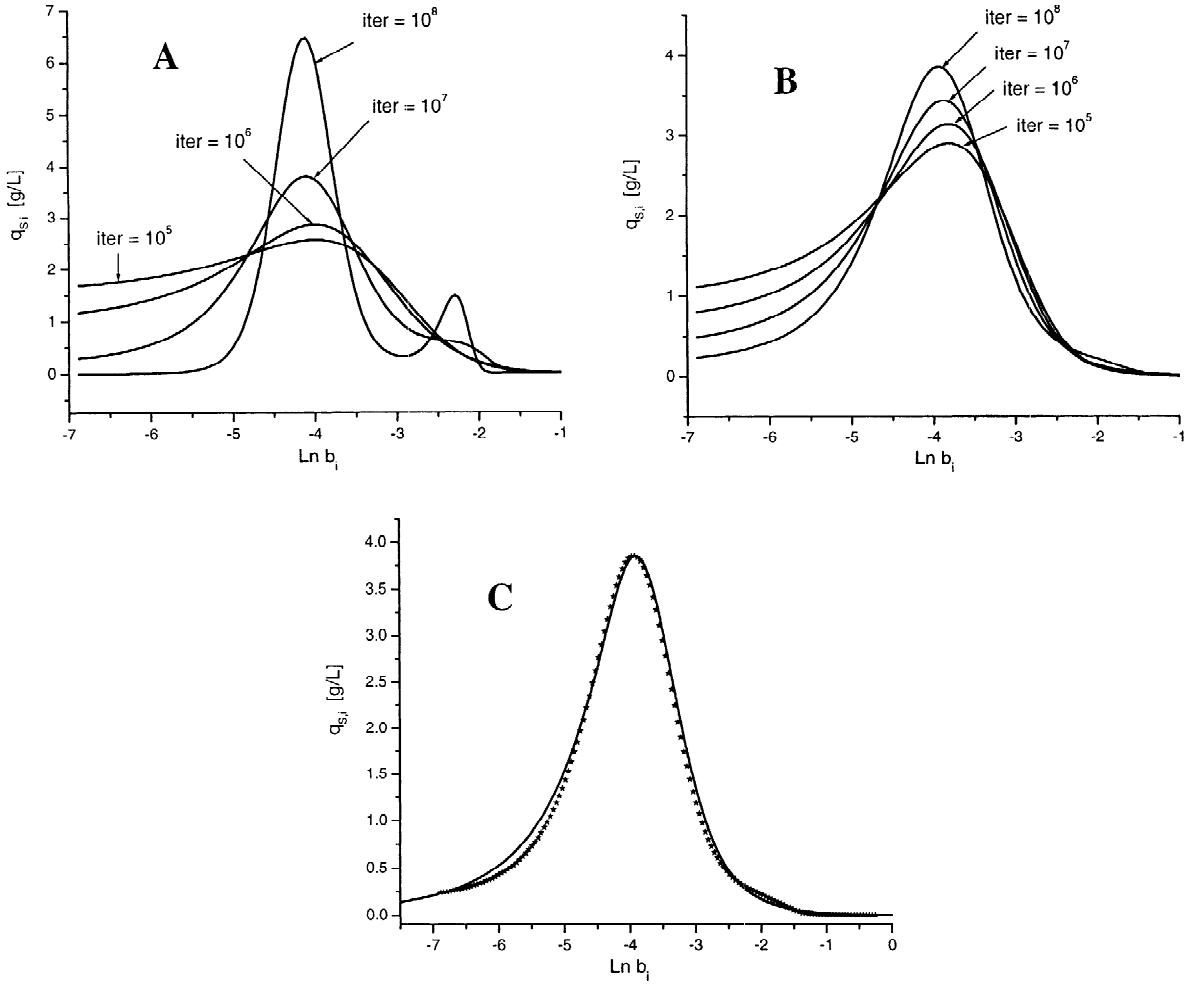

Fig. 11. AED of phenol on the packed Kromasil-C_{18} column with methanol–water (45:55, v/v) as the mobile phase. (A) AED calculated from 36 calculated adsorption data points assuming the Bi-Langmuir model whose parameters are listed in Table 2 (the values of q^* are truncated at the fifth decimal). (B) AED calculated from 36 calculated adsorption data points assuming the Toth model whose parameters are in Table 2 (the values of q^* are also truncated at the fifth decimal). The energy space is divided into 150 points. Four different numbers of iteration are used as indicated on the graph. (C) Comparison between the AED calculated in (B) for 10^8 iterations (stars plot) and this calculated using the analytical form of the Toth energy distribution presented in Eqs. (8)–(10) (thick solid line). $T = 295$ K.

shown in Fig. 11A,B. They demonstrate that the isotherm data derived from the Bi-Langmuir isotherm lead to a bimodal energy distribution and that those derived from the Toth isotherm lead to a unimodal energy distribution. The modes of these distributions have the correct energy. In other words, these calculations validate the EM calculation method since when applied to adsorption data deriving from a given energy distribution, the program gives numerical results that are consistent with this distribution.

The previous results suggest that the adsorption isotherm of phenol on Kromasil-C_{18} with methanol–water (45:55, v/v) as the mobile phase is best described by a bimodal Bi-Langmuir isotherm model. We can now recalculate a best fitting isotherm by imposing the new set of binding constants, b_1 and b_2, derived from the means of the two energy modes.

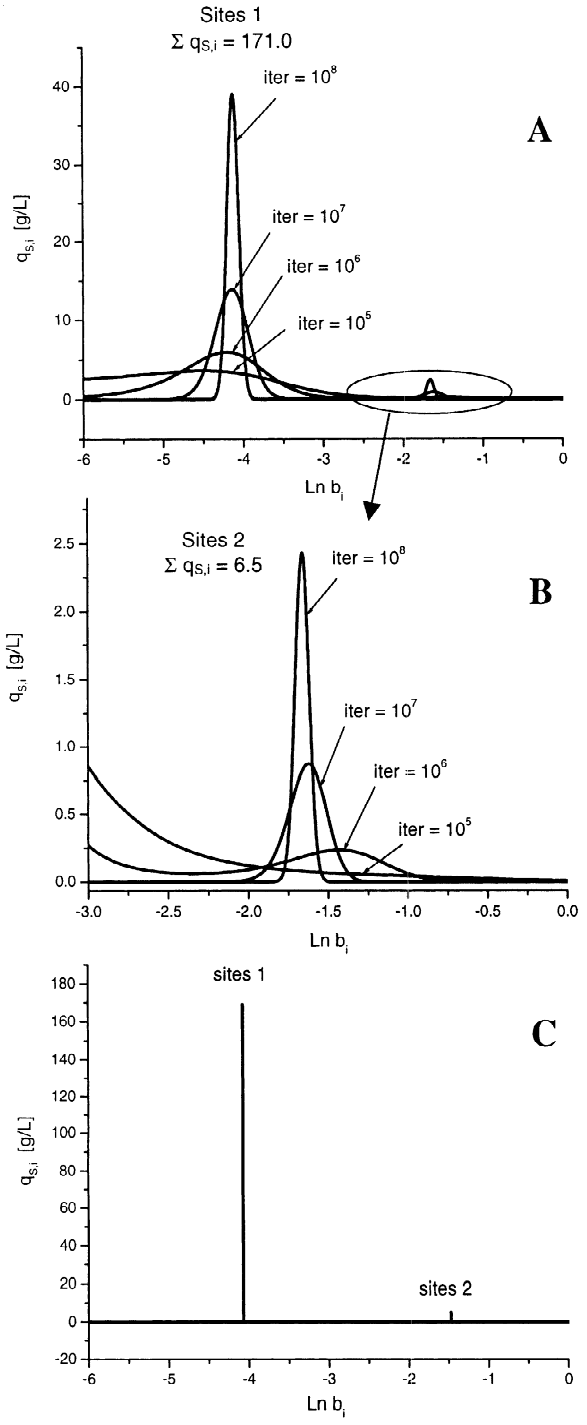

Fig. 12. Adsorption energy distribution (AED) of caffeine on the packed Kromasil-C_{18} column with methanol–water (30/70, v/v) as the mobile phase. (A) AED calculated from 36 experimental adsorption data points using the EM program (the values of q^* are truncated at the fifth decimal). The energy space is divided into 200 points. Four different numbers of iteration are used as indicated on the graph. (B) Zoom of the AED function corresponding to the high energy sites 2 of low saturation capacity. (C) Theoretical AED of the best Bi-Langmuir isotherm found by regression analysis of the same 36 adsorption data points. $T = 295$ K.

The nonlinear regression gives a new set of saturation capacities, 128.3 and 38.7 g/dm^3 for the low and the high energy sites, respectively. These values are nearly the same as those given by the EM algorithm (127.9 and 38.9 g/dm^3). The Fisher value is 118 600, only 30% less than the value obtained when all four isotherm parameters are optimized (Table 2). This new isotherm (not shown) could not be distinguished from the best one in Fig. 8. This isotherm gives calculated band profiles in excellent agreement with experimental ones as shown on Fig. 13.

The energy difference between the two types of sites is relatively small. From Eq. (3), we can derive that:

$$\ln(b_2) - \ln(b_1) = \frac{\varepsilon_{a,2} - \varepsilon_{a,1}}{RT} \quad (20)$$

Since the experiments were performed at 296 K, we have $RT = 2.46$ kJ/mol. The AED analysis gives a difference $\ln b_2 - \ln b_1$ of between 1.85 and 2.0. So, the energy difference of the two modes is about 5 kJ/mol. This suggests that there is not much difference in the nature of the interactions between the solute and the two different sites on the surface of the stationary phase. This difference is 10 times lower that the difference between the interaction energies of (*d*)-*N*-benzoylalanine and the selective and non-selective sites of bovine serum albumin immobilized on an ion-exchange resin [39]. Obviously, strong selective interactions take place on the enantioselective sites. In the case of a C_{18}-bonded, endcapped column, it is likely that dispersion interactions are responsible for the first type of sites. However, the energy difference is too small to suggest that the second of sites could be explained

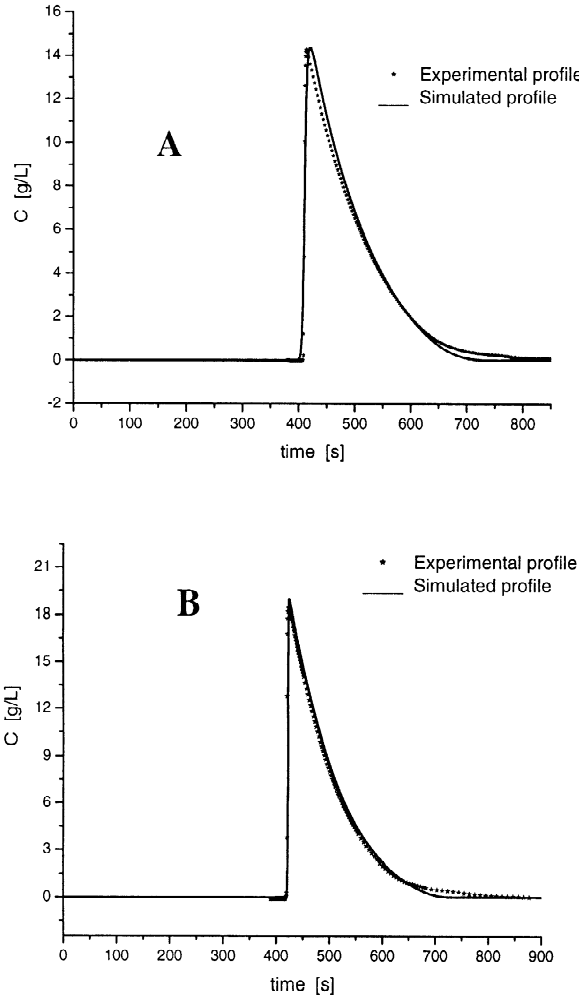

Fig. 13. Comparison between calculated (solid line) and experimental (stars plot) band profiles assuming the Bi-Langmuir model of adsorption. The parameters of the Bi-Langmuir are those derived from AED analysis. Stationary phase: packed Kromasil-C_{18} column. (A) Injection of a solution of phenol at 30 g/dm^3 during 54 s. $L_f \approx 10\%$. Mobile phase: methanol–water (45:55, v/v). (B) Injection of a solution of caffeine at 30.6 g/dm^3 during 54 s. $L_f \approx 10\%$. Mobile phase: (methanol–water (45:55, v/v). Flow rate 1 cm^3/min, $T = 295$ K.

by hydrogen-bond or ionic interactions. The relative importance of the saturation capacity of these last sites is too large to attribute them to the residual silanophilic groups on this endcapped C_{18} stationary phase.

4.3.2. Case of caffeine

Fig. 12A,B show the AED of caffeine, calculated with the 36 experimental data points. Again a bimodal energy distribution is observed. This time the program converges after fewer iterations, probably because of the larger distance between the energies of the two modes (0.01612 and 0.1903 g/dm^3, respectively) than in the case of phenol (0.00993 and 0.06338 g/dm^3), hence of their better resolution. There is an excellent agreement between the fitted parameters in Table 2 (see Fig. 12C) and those independently derived by the AED analysis. In this case, the error made on the Bi-Langmuir parameters is relatively low because the Scatchard plot (see Fig. 6) is strongly curved. The ratio b_2/b_1 is about twice larger than the one found in the case of phenol and the difference between the adsorption energies is about 6.5 kJ/mol. This difference is still insufficient to assume that the interactions of the solute with the two types of sites differ in nature. In contrast with the phenol case, the proportion of low ($q_{S,1}$) to high ($q_{S,2}$) energy sites is much larger, these values being, respectively, 171.0 and 6.5 g/dm^3. This means that either the number of high energy site is very low or that their access is difficult for caffeine molecules. This difference may be explained in part by the larger proportion of collapsed C_{18} chains due to the higher water concentration. In order to achieve a reasonable value for the retention factor, between 2 and 3, the mobile phase used for caffeine had 70% water instead of 45% in the one used for phenol.

In contrast with phenol again, the saturation capacities derived from a nonlinear regression of the isotherm data with fixed binding energies (171.3 and 6.5 g/dm^3) are very close to those obtained in the initial fit (168.9 and 5.2 g/dm^3). The calculated profiles (not shown) are hardly changed from those in Fig. 10.

5. Conclusion

Our results show that, in certain cases, several isotherm models can account almost equally well for isotherm data and for the profiles of overloaded elution bands. This happens for both phenol and caffeine on a Kromasil C_{18}-bonded silica column. Isotherm and band profiles are equally well ac-

counted for by the Toth and the Bi-Langmuir models, despite the fundamental differences between their physical principles and between their associated adsorption energy distributions. In such cases, more detailed investigations of the retention mechanism and of the thermodynamics of interactions between solute and stationary phase are warranted.

The calculation of the AED of the solutes involved, using the expectation maximization method, allowed a clear distinction between the properties of the two models. Because the EM algorithm does not require any assumption about the mathematical form of the isotherm but handles only the raw experimental data points, it affords characteristic properties of the AED with which the isotherm model must be compatible. In the case in point, both AED are bimodal which supports the Bi-Langmuir model and renders the Toth model implausible.

Investigations of this type should bring a deeper understanding of the nature and complexity of the interactions involved in liquid–solid adsorption. They may shed some new light on the vexing problem of the active sites that have not yet been clearly identified. The sensitivity of the method and its precision are probably insufficient at this stage. This may lead to the investigation of particular problems, such as those involved in chiral chromatography. Knowledge gained in this field may also be helpful in the design of models of competitive isotherms.

Acknowledgements

This work was supported in part by Grant DE-FG05-88-ER-13869 of the US Department of Energy and by the cooperative agreement between the University of Tennessee and the Oak Ridge National Laboratory. We thank Hans Liliedahl and Lars Torstensson (Eka Nobel) for the generous gift of the columns used in this work and for fruitful discussions.

References

[1] G. Guiochon, S. Golshan-Shirazi, A.M. Katti, in: Fundamentals of Preparative and Nonlinear Chromatography, Academic Press, Boston, MA, 1994.
[2] G. Guiochon, J. Chromatogr. A 965 (2002) 129.
[3] A. Felinger, G. Guiochon, J. Chromatogr. A 796 (1998) 59.
[4] I. Quiñones, J.C. Ford, G. Guiochon, Chem. Eng. Sci. 55 (2000) 909.
[5] D.M. Ruthven, in: Principles of Adsorption and Adsorption Processes, Wiley, New York, 1984.
[6] G. Schay, G. Szekely, Acta Chem. Hung. 5 (1954) 167.
[7] D.H. James, C.S.G. Phillips, J. Chem. Soc. (1954) 1066.
[8] E. Glueckauf, Trans. Faraday Soc. 51 (1955) 1540.
[9] E. Cremer, G.H. Huber, Angew. Chem. 73 (1961) 461.
[10] F.G. Helfferich, D.L. Peterson, J. Chem. Educ. 41 (1964) 410.
[11] C. Blümel, P. Hugo, A. Seidel–Morgenstern, J. Chromatogr. A 827 (1998) 175.
[12] D.H. Everett, Trans. Faraday Soc. 61 (1965) 2478.
[13] F. Riedo, E.Sz. Kovats, J. Chromatogr. 239 (1982) 1.
[14] I. Langmuir, J. Am. Chem. Soc. 40 (1918) 1361.
[15] D.S. Jovanovic, Colloid Polym. Sci. 235 (1969) 1203.
[16] I. Quinones, B. Stanley, G. Guiochon, J. Chromatogr. A 849 (1999) 45.
[17] M. Jaroniec, R. Madey, in: Physical Adsorption on Heterogeneous Solids, Elsevier, Amsterdam, 1988.
[18] R.J. Umpleby II, S.C. Baxter, Y. Chen, R.N. Shah, K.D. Shimizu, Anal. Chem. 73 (2001) 4584.
[19] J. Toth, in: Adsorption, Marcel Dekker, New York, 2002.
[20] B.J. Stanley, S.E. Bialkowski, D.B. Marshall, Anal. Chem. 65 (1993) 259.
[21] B.J. Stanley, G. Guiochon, J. Phys. Chem. 97 (1993) 8098.
[22] G. Zhong, P. Sajonz, G. Guiochon, Ind. Eng. Chem. (Res.) 36 (1997) 506.
[23] D. Graham, J. Phys. Chem. 57 (1953) 665.
[24] J. Toth, Acta Chem. Hung. 32 (1962) 31.
[25] J. Toth, Acta Chem. Hung. 69 (1971) 311.
[26] J. Toth, W. Rudzinski, A. Waksmundski, M. Jaroniec, S. Sokolowski, Acta Chem. Hung. 82 (1974) 11.
[27] M. Suzuki, in: Adsorption Engineering, Elsevier, Amsterdam, 1990.
[28] P.W. Danckwerts, Chem. Eng. Sci. 2 (1953) 1.
[29] K. Kaczmarski, M. Mazzotti, G. Storti, M. Morbidelli, Comput. Chem. Eng. 21 (1997) 641.
[30] K. Kaczmarski, Comput. Chem. Eng. 20 (1996) 49.
[31] K. Kaczmarski, D. Antos, J. Chromatogr. A 862 (1999) 1.
[32] P.N. Brown, A.C. Hindmarsh, G.D. Byrne, Procedure available from http://www.netlib.org.
[33] M. Kele, G. Guiochon, J. Chromatogr. A 855 (1999) 423.
[34] F. Gritti, W. Piatkowski, G. Guiochon, J. Chromatogr. A 978 (2002) 81.
[35] M. Pyda, B.J. Stanley, M. Xie, G. Guiochon, Langmuir 10 (1994) 1573.
[36] B.J. Stanley, G. Guiochon, Langmuir 10 (1994) 4278.
[37] B.J. Stanley, G. Guiochon, Langmuir 11 (1995) 1735.
[38] B.J. Stanley, J. Krance, A. Roy, J. Chromatogr. A 865 (1999) 97.
[39] S.C. Jacobson, G. Guiochon, J. Chromatogr. 600 (1992) 37.